Astronomy Letters, Vol. 31, No. 2, 2005, pp. 80–87. Translated from Pis'ma v Astronomicheskiĭ Zhurnal, Vol. 31, No. 2, 2005, pp. 91–98.

Leading Wave as a Component of the Spiral Pattern of the Galaxy

A. M. Mel'nik*

Sternberg Astronomical Institute, Universitetskiĭ pr. 13, Moscow, 119992 Russia

Received June 8, 2004

Abstract—The spiral pattern of the Galaxy, identified by analyzing the kinematics of young stars within 3 kpc of the Sun, is Fourier decomposed into spiral harmonics. The spiral pattern of the Galaxy is shown to be representable as a superposition of trailing and leading waves with interarm distances of $\lambda = 1.8 \pm 0.4$ and 4 ± 2 kpc, respectively. Shock waves are probably present only in the portions of the trailing spiral pattern where it crosses the crest of the leading wave. The small interarm distance of the trailing spiral wave ($\lambda = 1.8$ kpc) can be explained by its evolution—by the decrease in the interarm distance as the wave is displaced toward the inner Lindblad resonance. The Carina arm may be part of this resonance ring.

Key words: *Galaxy, spiral pattern, kinematics and dynamics, Fourier analysis.*

INTRODUCTION

An analysis of the velocity field for young stars (OB associations and Cepheids) revealed periodic variations in the radial and azimuthal components of the residual velocity along the Galactic radius vector with an amplitude of $f_R = f_\theta = 7 \pm 2$ km s^{-1} and a scale length of $\lambda = 2 \pm 0.2$ kpc (Mel'nik *et al.* 1999, 2001). We determined the kinematic locations of the Carina, Cygnus, and Perseus arms as the locations of the minima in the distribution of the radial residual velocity of OB associations. The identified arm fragments deviate from an ideal spiral pattern (smooth trailing spiral arms). The Carina arm ($R = 6.5$ kpc) is displaced from the Cygnus arm ($R = 6.8$ kpc) so that together they fall best on the leading spiral arm. The Perseus arm unexpectedly terminates, and we see its extension in the III quadrant neither from the kinematics of young stars nor from the increase in the density of young objects. An analysis of various spur generation mechanisms showed that the identified arm fragments are not spurs and are located near the minimum of the potential (Mel'nik 2003). The potential perturbation itself is probably not an ideal monochromatic spiral wave.

Following Kalnajs (1975), let us assume that the spiral pattern of the Galaxy is a superposition of several spiral waves and let us try to identify the various components of its spiral pattern. Kalnajs (1975) was the first to perform a Fourier analysis of the spiral pattern of a galaxy using the distribution of H II regions in the galaxy M 31. This analysis revealed a dominant one-armed leading spiral in it.

The spiral pattern of the Galaxy is difficult to analyze, because we do not have a complete picture of the distribution of young objects in its disk. On the other hand, only our Galaxy makes it possible to identify arm fragments kinematically. Therefore, we have not just a sample of spiral-arm indicators, but a sample of potential-minimum indicators.

FOURIER ANALYSIS OF THE GALACTIC SPIRAL PATTERN IN THE SOLAR NEIGHBORHOOD

The Method and Models

The complex spiral pattern of any galaxy can be represented as a superposition of spiral components with different numbers of arms m, and each m-component, in turn, can consist of several spiral waves with different pitch angles.

An elementary logarithmic spiral wave is defined by the equation

$$R = R_1 e^{\tan i(\theta - \theta_1)}, \qquad (1)$$

where i is the pitch angle, θ and θ_1 are the Galactocentric angles, and R and R_1 are the Galactocentric distances.

The amplitudes of the spiral oscillations in the distribution of N objects in the galactic plane can be determined from the relation

$$A(p, m) = \frac{1}{N} \sum_{j=1}^{N} e^{-i[m\theta_j + p \ln(R_j/R_0)]}, \qquad (2)$$

where $p = -m/\tan i$ (Kalnajs 1975; Considere and Athanossoula 1982).

*E-mail: anna@sai.msu.ru

Only the interarm distance λ and, in certain cases, the sense of arm winding can be reliably determined by analyzing the spiral pattern of the Galaxy within 3 kpc of the Sun. The number of spiral arms m and their mean pitch angle i remain indeterminate, although all three parameters are related by

$$|\tan i| = \frac{\lambda m}{2\pi R_0}, \qquad (3)$$

where R_0 is the Galactocentric distance.

The number of spiral arms cannot be determined by analyzing the distribution of young stars within 3 kpc of the Sun, because all of the m-components are very similar to one another, and the Fourier amplitude $A(p, m)$ actually depends only on the parameter p. Therefore, only the Fourier spectrum of the $m = 1$ spiral component is shown on the plots.

Let us consider two models of the Galactic spiral arms: In model 1, the spiral pattern of the Galaxy is represented by 15 real OB associations (Blaha and Humphreys 1989) that are located near the minimum in the distribution of the radial residual velocity V_R and that have $V_R < -5$ km s^{-1}. Table 1 lists these associations together with their heliocentric (r, l, b) and Galactocentric (R, θ) coordinates and the residual velocities V_R. Figure 1a shows the locations and residual velocities of these associations in the Galactic plane and the circular arcs that correspond to the minima in the distribution of the radial residual velocity. We excluded from our analysis the OB associations Sco OB4 ($l = 353°$, $r = 1.0$ kpc, $V_R = -15$ km s^{-1}) and HD 156154 ($l = 351°$, $r = 2.1$ kpc, $V_R = -16$ km s^{-1}); although their residual velocities are $V_R < -5$ km s^{-1}, they deviate greatly from the observed periodic pattern of the velocity field of young objects.

In model 2, the distribution of young objects is modeled in a ring. The points representing the OB associations are randomly scattered over the ring $R_0 - 2 < R < R_0 + 2$ kpc, except for the 3 kpc solar neighborhood where they concentrate toward the three arcs corresponding to three fragments of the spiral pattern (Fig. 1b). Table 2 lists the Galactocentric angles of the beginning and end marks of these arcs $\theta_{\min}$ and $\theta_{\max}$ and their Galactocentric distances $R_{\rm arm}$. The points in the arms are distributed uniformly, and their radial distribution is limited to the interval $R = R_{\rm arm} \pm 0.2$ kpc. The total number of points in the arms is equal to the number of points that would fell within the selected region of the ring (within 3 kpc of the Sun) if it were filled uniformly and randomly. Of the 2000 objects scattered over the ring, 250 objects, on average, fall within the selected region, and 40, 20, and 40% of these fall within the Carina, Cygnus, and Perseus arms, respectively.

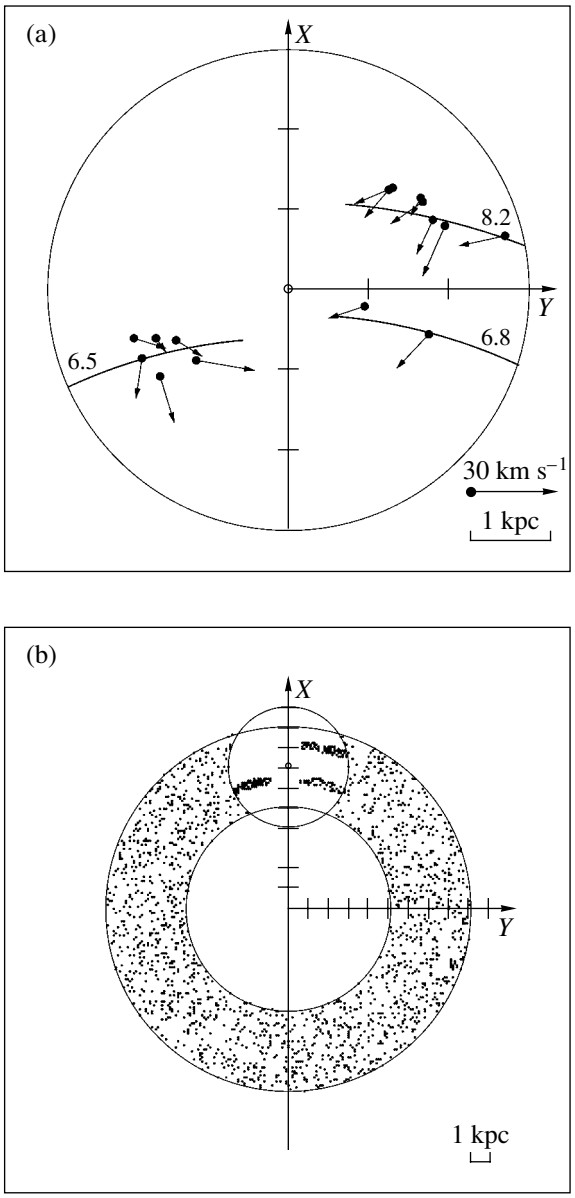

Fig. 1. Distribution of young objects in the Galaxy. (a) In model 1, the spiral pattern is represented by 15 real kinematically identified OB associations. The circular arcs correspond to the kinematic locations of the spiral arms. (b) In model 2, the young objects are randomly distributed in the ring $R_0 - 2 < R < R_0 + 2$ kpc, except for the 3 kpc solar neighborhood where they concentrate toward the identified fragments of the spiral pattern.

The modeled ring has a width of $\Delta R = \pm 2$ kpc, because we can ensure the completeness of our sample or, more specifically, the identification of all arm fragments in the solar neighborhood only in this interval. The tightly wound spiral pattern of the Galaxy forces us to be cautious, since the density of young objects changes much faster radially than azimuthally.

We assumed the distance to the Galactic center

Table 1. List of OB associations used in model 1

OB association	l	b	r, kpc	V_R, km s^{-1}	R, kpc	θ
Cyg OB3	72°.8	2°.0	1.8	−14.5	6.79	14°.93
Cyg OB9	77.8	1.8	1.0	−5.8	6.96	7.74
Cep OB1	104.2	−1.0	2.8	−8.7	8.23	19.08
Cas OB2	112.0	0.0	2.1	−19.0	8.13	13.89
Cas OB5	116.1	−0.5	2.0	−12.7	8.18	12.73
Cas OB7	123.0	1.2	2.0	−10.3	8.36	11.61
Cas OB1	124.7	−1.7	2.0	−6.8	8.41	11.31
Per OB1	134.7	−3.2	1.8	−7.8	8.49	8.81
Cas OB6	135.0	0.8	1.8	−11.2	8.43	8.44
Coll 228	287.6	−1.0	2.0	−6.6	6.77	−16.42
Car OB2	290.4	0.1	1.8	−5.6	6.69	−14.20
Cru OB1	294.9	−1.1	2.0	−13.5	6.51	−16.23
NGC 3766	294.1	−0.0	1.5	−7.3	6.62	−12.15
Cen OB1	304.2	1.4	1.9	−16.8	6.23	−14.77
Hogg 16	307.5	1.4	1.5	−7.4	6.32	−10.52

to be $R_0 = 7.1$ kpc (Dambis *et al.* 1995; Glushkova *et al.* 1998) and shorten the distance scale for OB associations given by Blaha and Humphreys (1989) by 20% to reduce it to the so-called short distance scale (Dambis *et al.* 2001; Sitnik and Mel'nik 1996).

RESULTS

The heavy line in Fig. 2 indicates the Fourier decomposition of the distribution of 15 OB associations over the Galactic plane into logarithmic spiral waves. The parameter p, which characterizes the interarm distance $\lambda = 2\pi R_0/|p|$ and the sense of arm winding, is along the horizontal axis; $p > 0$ and $p < 0$ correspond to the trailing and leading arms, respectively. The absolute values of the amplitudes of the one-armed spiral waves $|A(p, 1)|$ are along the vertical axis. Figure 2 clearly shows three maxima. The leftmost and rightmost outside maxima at $p = -28$ and $p = +24$ correspond to a tightly would spiral pattern with $\lambda = 1.8 \pm 0.4$ kpc. The Fourier spectrum of the tightly wound spiral arm consists of a superposition of the leading and trailing components, since we consider only a small region where the tightly wound spiral arms are indistinguishable from circular arcs. The circular arc is decomposed into a superposition of leading and trailing spiral waves with approximately equal amplitudes and pitch angles $|i|$. The central maximum in Fig. 2 stems from the fact that we are dealing with a sample with a highly asymmetric distribution about the Galactic center. Indeed, all of the associations in model 1 are located within 3 kpc of the Sun rather than distributed over the entire Galactic disk. Such a cluster of objects corresponds to a spiral wave with an infinite pitch angle ($p = 0$). The width

Table 2. Parameters of the spiral pattern used in model 2

Arm fragments	$\theta_{\min}$	$\theta_{\max}$	$R_{\rm arm}$, kpc
Carina	−25°	−5°	6.5
Cygnus	+5	+25	6.8
Perseus	+5	+21	8.2

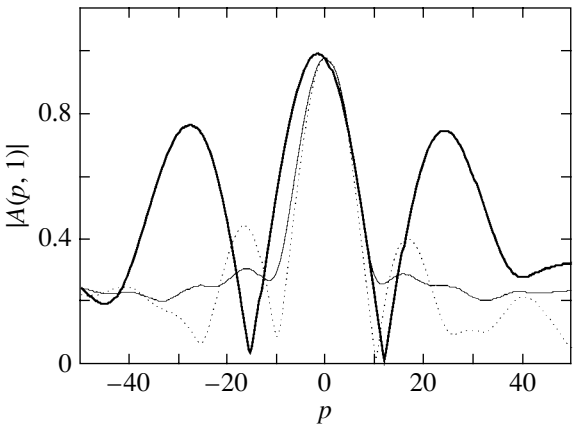

Fig. 2. Fourier decomposition of the distribution of 15 real OB associations into spiral harmonics (heavy line); the Fourier spectrum of one random distribution of 15 objects (dotted line), and the Fourier decomposition of the random distribution averaged over 100 samples (thin line).

of the central maximum depends on the size of the cluster: the smaller the clump, the wider the central maximum.

The dotted line in Fig. 2 indicates the Fourier decomposition for 15 objects randomly distributed in the 3 kpc solar neighborhood or, to be more precise, in the region where the circle $r = 3$ kpc and the ring $R_0 - 2 < R < R_0 + 2$ kpc intersect. We clearly see the maximum at $p = 0$ and the amplitude fluctuations on both sides of it. The thin line in Fig. 2 indicates the Fourier decomposition of a random distribution of 15 objects in the above solar neighborhood averaged over 100 samples. The Fourier spectrum of one random distribution agrees well with the mean spectrum in the central region ($p = 0$), where the amplitude fluctuations are small. The mean spectrum of the random distribution is a symmetric function relative to which we clearly see the central maximum of the Fourier decomposition of the real sample to be displaced toward the negative p, i.e., toward the leading waves. No random fluctuations can explain this displacement.

Let us assume the mean amplitude of the random distribution of 15 objects to be a background. We are interested in the difference $\Delta A(p, 1)$ between the Fourier amplitude for the real sample and the background. The heavy line in Fig. 3a indicates the absolute value of this difference $|\Delta A(p, 1)|$. We clearly see three maxima at $p = -28$, $p = +24$, and $p = -10$. The maximum at $p = -10$ points to the presence of a leading wave with a large interarm distance of $\lambda = 4.5 \pm 2.0$ kpc in the morphology of the Galactic spiral pattern.

The rms deviation of the Fourier amplitude of one random sample from the background is 0.12 and does

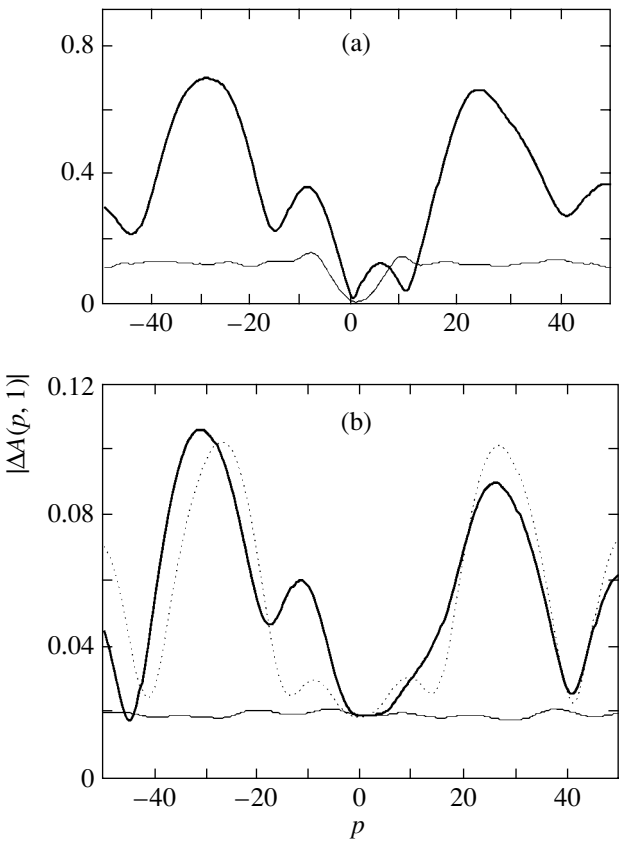

Fig. 3. (a) Absolute value of the difference between the Fourier amplitude calculated for the real distribution and the mean Fourier amplitude for a random distribution of 15 objects (heavy line); the rms deviation of the amplitude of a random sample from the background (thin line); we clearly see these three maxima at $p = -28$, $p = +24$, and $p = -10$. (b) The Fourier decomposition of the distribution of young objects in model 2 (heavy line); the Fourier decomposition for the fragments of an ideal spiral pattern (dotted line); the mean amplitude of the random distribution of young objects in the ring thin line; we clearly see three maxima at $p = -31$, $p = +26$, and $p = -12$.

not depend on p, except for the central region where it is close to zero (the thin line in Fig. 3a). The maxima at $p = -28$, $p = +24$, and $p = -10$ are not the result of random background fluctuations at the 99% confidence level.

Any Fourier decomposition contains high-order harmonics that, in our case, correspond to the increasingly tightly would spiral patterns at $p = 2p_0$, $3p_0$, $4p_0, \ldots$, where p_0 is the fundamental harmonic ($|p_0| = 26$). Our Fourier spectra also have high-order harmonics, but they are outside our figures.

It is interesting to note the causes of such deep and sharp minima in the Fourier decomposition of the real sample (Fig. 2). They correspond to a wave with an interarm distance ($|p| = 13$) that is twice the main tightly wound spiral pattern ($|p_0| = 26$). Since such a wave would inevitably arrive in opposite phases at the

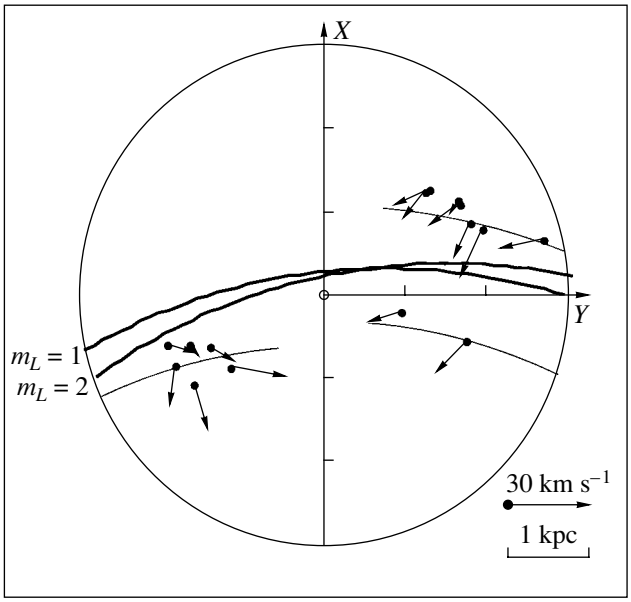

Fig. 4. Most probable locations of the leading wave with $\lambda = 4.5$ kpc and a pitch angle of $i = 6^\circ$ and $i = 12^\circ$ for the one-armed ($m_L = 1$) and two-armed ($m_L = 2$) models of the leading wave. In both cases, the leading wave in the solar neighborhood lies nearly halfway between the combined Carina–Cygnus and Perseus arm fragments.

Perseus arm and at the combined Carina–Cygnus arm fragment, it is absent in the spectrum.

The heavy line in Fig. 3b indicates the Fourier decomposition of the distribution of young objects in model 2. We clearly see three maxima at $p = -31$, $p = +26$, and $p = -12$ that correspond to a tightly wound spiral pattern with an interarm distance of $\lambda = 1.6 \pm 0.5$ kpc and a leading wave with $\lambda = 3.8 \pm 2.0$ kpc. No central maximum emerges in model 2, because any two halves of the Galaxy contain almost equal numbers of points. The scales of the vertical axes of models 1 and 2 differ by a factor of 10. However, we are interested not in the absolute values, but in the form of the Fourier decomposition. The Fourier decomposition of the random distribution of young objects throughout the ring consists of random amplitude fluctuations that do not exceed 0.06. The mean amplitude of these fluctuations is $|A(p, 1)| = 0.02$ (the thin line in Fig. 3b). None of the three maxima at $p = -31$, $p = +26$, and $p = -12$ is the result of random fluctuations in the distribution of young objects at the 99% confidence level.

To understand why the leading wave appears, let us consider the Fourier decomposition of an ideal spiral pattern in the solar neighborhood. The model of an ideal spiral pattern is a modification of model 2 (Fig. 1b). The difference is that objects within 3 kpc of the Sun concentrate toward two rather than three arm fragments that do not terminate anywhere within this region. The arms are in the shape of circular arcs and are located at the Galactocentric distances of the Carina ($R = 6.5$ kpc) and Perseus ($R = 8.2$ kpc) arms. The model is symmetric about the X-axis. Both arms contain equal numbers of objects.

The dotted line in Fig. 3b indicates the Fourier decomposition of an ideal spiral pattern. It exhibits two large maxima at $p = \pm 26$ and two barely visible, but unremovable maxima at $p = \pm 9$. The large maxima correspond to the main tightly wound spiral pattern, while the small maxima correspond to spiral waves with an interarm distance that is a factor of 3 larger than the distance between the Perseus and Carina arms. These waves emerge, since the circumference under consideration includes two arm fragments and the interarm space between them. Three halves of the main wave, $3\lambda_0/2$, can be covered by one half of the other wave, $\lambda_1/2$. This wave describes the behavior of all objects within 3 kpc of the Sun, without separating them between the arms, and its maximum must be located approximately halfway between the arms.

The detected leading wave with $\lambda = 4 \pm 2$ kpc is of the same nature. It describes the behavior of all objects within 3 kpc of the Sun. Figure 4 shows the most probable location of the leading arm. It has a pitch angle of $i = 6^\circ$ and $i = 12^\circ$ for the one-armed ($m_L = 1$) and two-armed ($m_L = 2$) models of the leading wave, respectively. In both cases, the leading arm intersects the X axis at a Galactocentric distance of $R = 7.4 \pm 0.5$ kpc (for the assumed Galactocentric distance of the Sun $R_0 = 7.1$ kpc); i.e., it lies exactly halfway between the combined Carina–Cygnus fragment and the Perseus arm.

Both defects of the spiral pattern—the displacement of the Carina and Cygnus arm fragments toward the leading spiral and the absence of the Perseus arm extension in the III quadrant—give rise to a leading wave. However, the termination of the Perseus arm makes a much larger contribution to the leading wave.

Both models yield similar results. However, the following trend clearly shows up in model 2. The leading wave tends to have an interarm distance that is twice λ of the tightly wound spiral pattern. This is because we actually have two fragments of the spiral pattern: the combined Carina–Cygnus fragment and the Perseus arm. In order to weaken the second fragment without weakening the first, the additional wave must have an interarm distance that is twice that of the main tightly wound spiral wave. To weaken the Perseus arm in the III quadrant without weakening it significantly in the II quadrant, the additional spiral wave must be a leading one.

Thus, the distribution of OB associations within 3 kpc of the Sun can be represented as a superposition

of two spiral components: a tightly wound spiral wave with an interarm distance of $\lambda = 1.8 \pm 0.4$ kpc and a leading arm with an interarm distance of $\lambda = 4 \pm 2$ kpc.

How can the detection of other more distant fragments of the tightly wound spiral pattern change the parameters of the leading wave? The leading wave proved to be most sensitive to the asymmetry of the new possible arm fragments about the X axis. The amplitude of the leading wave would increase only if, for example, the new distant fragment detected in the outer Galaxy were as asymmetric about the X axis as the Perseus arm (i.e., more objects would be located in the II quadrant than in the III quadrant; Fig. 1b). In contrast, in the inner Galaxy a distant fragment must contain more objects in the IV quadrant than in the I quadrant to amplify the leading wave. In general, the asymmetry in the distribution of young objects required to amplify the leading wave agrees with the asymmetry in the H I distribution in the Galaxy (Blitz and Spergel 1991).

HOW DOES EACH SPIRAL COMPONENT MANIFEST ITSELF IN THE KINEMATICS AND DISTRIBUTION OF YOUNG STARS?

While analyzing the locations of the spiral arm fragments identified by the kinematics of young stars, we implicitly assumed that the additional components of the spiral pattern would not disrupt the periodic pattern of the velocity field of young stars. The large interarm distance of the leading component agrees well with this assumption. Indeed, the velocity perturbation amplitudes f_R and f_θ for young stars must be proportional to λ^{-1} (Lin *et al.* 1969). Consequently, even if the other parameters of the spiral pattern (the perturbations of the potential and the locations with respect to the corotation radius) are equal, the velocity perturbation amplitudes for the leading wave must be a factor of 2 lower than those for the tightly wound wave. In general, the velocity perturbations for young stars can be explained without invoking the leading wave.

The tightly wound spiral wave was first found by analyzing the kinematics of young stars (Mel'nik *et al.* 1999, 2001). In the Fourier spectrum, it is represented by a superposition of leading and trailing spiral waves. However, the kinematics of young objects strongly suggests that the tightly wound spiral pattern is a trailing wave.

The sense of winding is determined by the following. The radial components of the mean residual velocities for the young stars that concentrate in the Cygnus and Perseus arms are directed toward the Galactic center, while their azimuthal components are opposite to the sense of Galactic rotation. Three conclusions can be drawn from this: First, the Cygnus and Perseus arm fragments represent a trailing spiral pattern. Second, the Cygnus and Perseus arm fragments are located within the corotation circle. Third, the coincidence of the minima in the distributions of radial and azimuthal residual velocities is indicative of the presence of a shock (see Mel'nik (2003) for more detail).

A problem arises with the Carina arm. We observe an enhanced concentration of young stars in all three arm fragments: the Perseus, Cygnus, and Carina arms. However, in the Carina arm, we find no significant variations in the azimuthal residual velocity across the arm, while the radial residual velocity exhibits a well-defined minimum (see Fig. 5 in Mel'nik *et al.* 2001). The absence of an azimuthal velocity gradient across the Carina arm may be attributable to the distance errors that can effectively blur the variations exactly in the azimuthal velocity (see Mel'nik (2003) for more detail). However, this defect can also have a different cause, one which is discussed in the next section.

The leading wave clearly shows up only in the relative location of the spiral arm fragments. Indeed, all three fragments of the Carina, Cygnus, and Perseus arms can be imagined as lying on a broad leading spiral arm. This distribution can stem from the fact that the star formation is more intense in the portions of the trailing spiral arms where they cross the crest of the leading wave. Shocks seem to be also present only in these arm portions. This behavior can be explained using the model of Roberts and Hausman (1984), in which the motion of particle clouds is considered in a perturbed potential. The enhanced surface density of the disk in these portions must cause additional crowding of the cloud orbits and increase the cloud–cloud collision frequency, which, in turn, can give rise to shocks.

Thus, the presence of a leading wave in the Galactic disk allows certain deviations from an ideal spiral pattern to be explained. The leading wave emerges mainly because the Perseus arm weakens in the III quadrant. The simplest explanation of the weakening of the Perseus arm consists in a decrease of the disk surface density in this region.

EVOLUTION OF THE GALACTIC SPIRAL PATTERN

Another peculiarity of the Galactic spiral pattern is the unusually small interarm distance of the trailing spiral wave ($\lambda = 1.8 \pm 0.4$ kpc), which is rarely observed in other galaxies. The tightly wound spiral pattern of our Galaxy may appear as a ring or part of it from a large distance.

The two peculiarities of the Galactic spiral pattern—the presence of shock and a tightly wound spiral pattern—force us to abandon the theory of modes, which is attractive in that it can ensure a quasi-steady state. The large energy losses in the shock require an efficient spiral wave amplification mechanism from the model to ensure a quasi-steady state. However, this mechanism (swing amplification) gives rise only to open spiral patterns (Toomre 1981; Athanossoula 1984). The observed tightly wound spiral pattern is probably not a mode and must evolve along the Galactic radius vector.

Toomre (1969) showed that over several galaxy rotations, the short trailing spiral wave displaces from the corotation region to the inner Lindblad resonance. During this displacement, the distance between the turns of the spiral wave decreases, while the density and velocity perturbations of the young stars remain high for a long period of time (Toomre 1969, 1977; Lin 1970). The trailing spiral wave observed in the Galaxy may be located near the inner Lindblad resonance. The unusually small interarm distance of the trailing wave can be explained by its evolution: the decrease in the interarm distance as the wave displaces toward the inner Lindblad resonance.

The Carina arm may be part of this resonance ring. First, we see no tightly wound spiral arms within the region bounded by the Carina arm. The kinematics of the Sagittarius arm differs markedly from that of the Perseus, Cygnus, and Carina arms (see Mel'nik *et al.* (2001) for more detail), and it cannot be considered to be a fragment of the same spiral wave. Second, the ring geometry of the Carina arm could in principle explain the absence of cross-arm variations in the azimuthal residual velocity.

The superposition of the trailing and leading spiral arms found in our Galaxy is not unique. The galaxy M 31 exhibits a similar pattern with the leading and trailing arms having interarm distances of 6 and 4 kpc, respectively (Considere and Athanossoula 1982). The main difference is that the interarm distance of the trailing wave in the Galaxy is a factor of about 2 smaller. In addition, the leading wave in the Andromeda galaxy is known to be one-armed. No such information is available for our Galaxy.

CONCLUSIONS

The spiral pattern of the Galaxy identified by the kinematics of young stars within 3 kpc of the Sun was Fourier decomposed into spiral harmonics. We showed that the spiral pattern could be represented as a superposition of trailing and leading waves with interarm distances of $\lambda = 1.8 \pm 0.4$ and 4 ± 2 kpc, respectively.

The presence of a leading wave in the Galactic disk makes it possible to explain certain deviations from an ideal spiral pattern. The leading wave clearly shows up only in the large-scale distribution of young objects and has virtually no effect on their kinematics. Shocks seem to exist only in the portions of the trailing spiral pattern where it intersects the crest of the leading wave. An enhanced surface density of the disk in these portions must cause additional crowding of the cloud orbits and increase the cloud–cloud collision frequency, which, in turn, can give rise to shocks (Roberts and Hausman 1984).

The small interarm distance of the trailing spiral wave ($\lambda = 1.8$ kpc) can be explained by its evolution: the decrease in the interarm distance as the wave displaces toward the inner Lindblad resonance. The Carina arm may be part of this resonance ring. It may well be that there is a spiral pattern in the region bounded by the Carina arm, but this is a different spiral pattern.

The leading wave in our Galaxy could be regenerating the trailing spiral pattern via the swing amplification mechanism (Goldreich and Lynden-Bell 1965; Julian and Toomre 1966; Toomre 1981). However, it remains unclear why it emerges.

ACKNOWLEDGMENTS

I am grateful to A.V. Zasov, I.I. Pasha, A.S. Rastorgouev, Yu.N. Efremov, and A.K. Dambis for interesting discussions and useful remarks. This work was supported by the Russian Foundation for Basic Research (project nos. 02-02-16677 and 03-02-16288), the Council for the Program of Support for Leading Scientific Schools (project no. NSh.389.2003.2), and the State Science and Technology Astronomy Program.

REFERENCES

1. E. Athanassoula, Phys. Rep. **114**, 319 (1984).
2. C. Blaha and R. M. Humphreys, Astron. J. **98**, 1598 (1989).
3. L. Blitz and D. N. Spergel, Astrophys. J. **370**, 205 (1991).
4. S. Considere and E. Athanassoula, Astron. Astrophys. **111**, 28 (1982).
5. A. K. Dambis, A. M. Mel'nik, and A. S. Rastorguev, Pis'ma Astron. Zh. **21**, 331 (1995) [Astron. Lett. **21**, 291 (1995)].
6. A. K. Dambis, A. M. Mel'nik, and A. S. Rastorguev, Pis'ma Astron. Zh. **27**, 68 (2001) [Astron. Lett. **27**, 58 (2001)].
7. E. V. Glushkova, A. K. Dambis, A. M. Mel'nik, and A. S. Rastorguev, Astron. Astrophys. **329**, 514 (1998).
8. P. Goldreich and D. Lynden-Bell, Mon. Not. R. Astron. Soc. **130**, 125 (1965).

9. W. H. Julian and A. Toomre, Astrophys. J. **146**, 810 (1966).
10. A. J. Kalnajs, *La Dynamique des Galaxies Spirales, Coll. Int. CNRS No. 241*, Ed. by L. Weliachew (Editions du Centre National de la Recherche Scientifique, Paris, 1975), p. 103.
11. C. C. Lin, *The Spiral Structure of Our Galaxy, IAU Symp. 38*, Ed. by W. Becker and G. Contopoulos (Reidel, Dordrecht, 1970), p. 377.
12. C. C. Lin, C. Yuan, and F. H. Shu, Astrophys. J. **155**, 721 (1969).
13. A. M. Mel'nik, Pis'ma Astron. Zh. **29**, 349 (2003) [Astron. Lett. **29**, 304 (2003)].
14. A. M. Mel'nik, A. K. Dambis, and A. S. Rastorguev, Pis'ma Astron. Zh. **25**, 602 (1999) [Astron. Lett. **25**, 518 (1999)].
15. A. M. Mel'nik, A. K. Dambis, and A. S. Rastorguev, Pis'ma Astron. Zh. **27**, 611 (2001) [Astron. Lett. **27**, 521 (2001)].
16. W. W. Roberts and M. A. Hausman, Astrophys. J. **277**, 744 (1984).
17. T. G. Sitnik and A. M. Mel'nik, Pis'ma Astron. Zh. **22**, 471 (1996) [Astron. Lett. **22**, 422 (1996)].
18. A. Toomre, Astrophys. **158**, 899 (1969).
19. A. Toomre, Annu. Rev. Astron. Astrophys. **15**, 437 (1977).
20. A. Toomre, *The Structure and Evolution of Normal Galaxies*, Ed. by S. M. Fall and D. Lynden-Bell (Cambridge Univ. Press, Cambridge, 1981), p. 111.

Translated by V. Astakhov